RESEARCH ARTICLE

NANO · MICRO small
www.small-journal.com

Evaluation of the Biocompatibility of Poly(benzimidazobenzophenanthroline)(BBL) Polymer Films with Living Cells

Claudia Latte Bovio, Paola Campione, Han-Yan Wu, Qifan Li, Ana De La Fuente Durán, Alberto Salleo, Simone Fabiano, Grazia Maria Lucia Messina,* and Francesca Santoro**

The integration of organic electronic materials with biological systems to monitor, interface with, and regulate physiological processes is a key area in the field of bioelectronics. Central to this advancement is the development of cell-chip coupling, where materials engineering plays a critical role in enhancing biointerfacing capabilities. Conductive polymers have proven particularly useful in cell interfacing applications due to their favorable biophysical and chemical properties. However, n-type conductive polymers remain underexplored, primarily due to their limited long-term stability. In this study, it is demonstrated that the conductive polymer poly(benzimidazobenzophenanthroline) (BBL), commonly used in organic electronic devices, can effectively support neuronal cell viability and spreading, both as a bare cell culture material and when coated with exracellular matrix proteins. This work provides a preliminary validation of BBL's potential for future integration into bioelectronic devices and in biointerfacing.

1. Introduction

Bioelectronics is a field that focuses on the direct interaction between electronic systems and biological entities to monitor physiological processes.[1–3] A key area of interest involves coupling electrogenic cells, such as neurons and cardiomyocytes, with electronic devices to investigate transient electrical signals (action potentials). These signals are facilitated by ion-specific channels and pumps across cell membranes, where the movement of ions generates voltage changes that transition cells from a resting to an excited state, potentially propagating action potentials to neighboring cells.[4–6]

In this context, conductive polymers (CPs) have found significant applications in enabling functional organic optoelectronic interfaces with electrogenic cells for monitoring and stimulation, triggering specific cellular responses and outgrowth.[6–8] A wide range of organic bioelectronic platforms utilize p-type (hole-transporting) materials, often incorporating additives to ensure long-term stability in aqueous environment for sustained cell interfacing.[9,10] Notably, materials such as poly(3,4-ethylenedioxythiophene):polystyrene sulfonate (PEDOT:PSS),

C. Latte Bovio, F. Santoro
Tissue Electronics
Istituto Italiano di Tecnologia
Naples 80125, Italy
E-mail: f.santoro@fz-juelich.de

C. Latte Bovio
Dipartimento di Chimica
Materiali e Produzione Industriale
Università di Napoli Federico II
Naples 80125, Italy

P. Campione, G. M. L. Messina
Laboratory for Molecular Surface and Nanotechnology (LAMSUN)
Department of Chemical Sciences
University of Catania. and CSGI
Viale A. Doria, 6, Catania 95125, Italy
E-mail: gml.messina@unict.it

H.-Y. Wu, Q. Li, S. Fabiano
Laboratory of Organic Electronics Department of Science and Technology
Linköping University
Norrköping SE-60174, Sweden
E-mail: simone.fabiano@liu.se

A. De La Fuente Durán, A. Salleo
Department of Materials Science and Engineering
Stanford University
Stanford, CA 94305, USA

F. Santoro
Faculty of Electrical Engineering and IT
RWTH
52074 Aachen, Germany

F. Santoro
Institute for Biological Information Processing-Bioelectronics
Forschungszentrum Juelich
52428 Julich, Germany

The ORCID identification number(s) for the author(s) of this article can be found under https://doi.org/10.1002/smll.202404451

DOI: 10.1002/smll.202404451

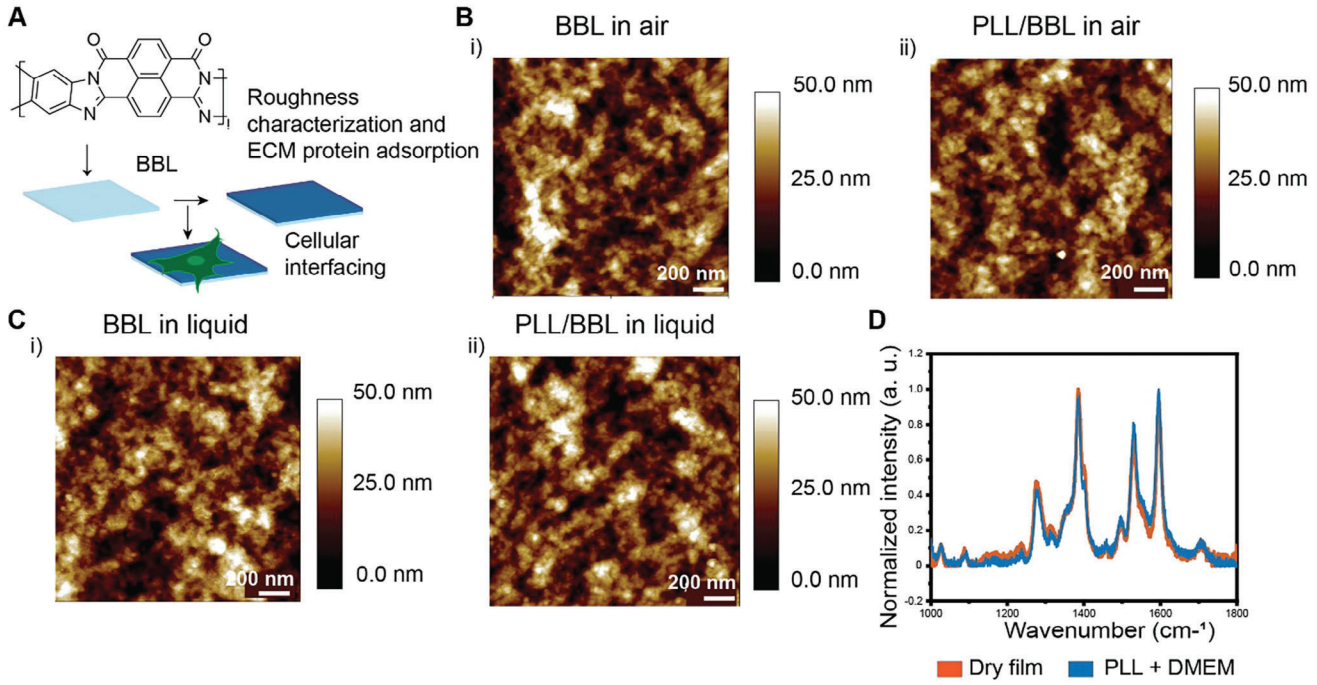

Figure 1. Characterization of BBL films surface and stability in cell media conditions. A) Schematics representing BBL film functionalization and biointerfacing, B) tapping mode atomic force micrograph of BBL film (acquisition area 2 µm x 2 µm) representing the surface morphology by height image in dry condition (in air) for i) pristine BBL and ii) PLL coated BBL. C) tapping mode atomic force micrograph of BBL film (acquisition area 2 µm x 2 µm) representing the surface morphology in liquid condition by height image for i) pristine BBL and ii) PLL coated BBL. D) Raman spectra acquired for a dry, neutralized BBL film and a neutralized BBL film incubated in PLL and submerged in cell media.

poly(3-hexylthiophene-2,5-diyl) (P3HT), and polyaniline (PANI), in various architectures—including particles, planar 2D films, and scaffold-based devices—have demonstrated diverse effects on cellular behavior, such as neuronal polarization, network development, and electrical signal propagation.[11–14] N-type (electron-transporting) materials have also recently gained attention in the bioelectronic fields, driven by their use in high-performance bio-/physical-/chemical sensor.[10,15] However, they remain underexplored in neuronal interfaces.[16]

Among the various n-type materials reported to date, the ladder-type benchmark polymer poly(benzimidazobenzophenanthroline) (BBL) stands out as a highly promising mixed ionic-electronic conductor for organic bioelectronic applications. Its highly planar and rigid backbone facilitates efficient intramolecular charge transport, leading to high carrier mobility.[17,18] Additionally, the side chain-free polymer backbone contributes to its high volumetric capacitance.[19,20] When used as the channel material in organic electrochemical transistors (OECTs), BBL imparts high transconductance and exhibits remarkable stability in aqueous media.[21] This property has enabled the development of high-performance amplifiers[22,23] for efficient bio-signal transduction and artificial spiking neurons[24,25] capable of replicating key biological neural features and stimulating biological neurons in living organisms. The successful demonstration of these capabilities suggests that BBL has potential for developing event-based sensors.

These sensors could transduce biochemical signals into stimuli to activate biological neurons, facilitating closed-loop physiological regulation. However, integrating these devices within or near the human body still requires a careful evaluation of the biocompatibility of BBL.

In this study, we explored the potential of BBL as a platform for neuronal cell cultures, both with and without poly-L-lysine (PLL) coating. We examined the morphology and stability of BBL films in cell culture medium using atomic force microscopy and Raman spectroscopy and investigated the films' interface with extracellular matrix protein coatings—designed to promote cell growth—using quartz crystal microbalance. Furthermore, we assessed the material's biocompatibility and ability to support cell outgrowth through optical and electron microscopy.

This work represents the first validation of BBL for use in neuroelectronic devices, highlighting its potential for long-term interfacing and adaptable coupling properties.

2. Results and Discussion

The morphology of both pristine BBL films and PLL-coated BBL was analyzed using atomic force microscopy (AFM) (**Figure 1A**), in air and in phosphate buffered saline solution (PBS) to simulate physiological conditions. As shown in Figure 1Bi, the height images of the pristine BBL thin film reveal the formation of a homogeneous polymer layer with an average surface roughness of 9.3 ± 1.0 nm (Table S1, Supporting Information). The 3D image (Figure S1Ai, Supporting Information) provides a more detailed view of the surface topography, highlighting the nanoscale features of the BBL film.

In Figure 1Bii, the morphology of the PLL-coated BBL, after a 1 h incubation with PLL solution, shows a surface similar to that of the pristine BBL film. This is confirmed by the roughness value, which is slightly lower but within the error range at 8.5 ± 0.7 nm (Table S1, Supporting Information). Although the average roughness values of both BBL and PLL-coated BBL are comparable, the 3D image in Figure S1Aii (Supporting Information), reveals a slightly sharper surface texture in the PLL-coated BBL, compared to the smoother appearance of the pristine BBL. This difference is likely due to the adsorption of PLL at the interface.

The comparison of AFM morphological analysis conducted in both air and liquid (Figures 1B,C and 3D images in Figure S1A,B, Supporting Information, scanning electron microscopy (SEM) images in Figure S2A,B, Supporting Information) confirms the homogeneous surface morphology, demonstrating the stability of the films in both environments. In liquid conditions the difference in average roughness between the uncoated (Figure 1Ci) and coated samples (Figure 1Cii) is negligible than in dry conditions (Table S1, Supporting Information). This indicates that the protein coating, in either condition, does not significantly alter the surface roughness, which could be beneficial for cell–surface interactions, and the films are stable in both the analyzed environments showing no sign of detachment. Furthermore, the surface mechanical properties at the nanometer scale have been measured by means of nanoindentation with AFM. From the collected force-distance curves, by fitting the slope in the elastic region with the Derjaguin, Muller and Toporov (DMT) model, Young's modulus value has been obtained for BBL film (567 ± 15.7 MPa), suggesting a stiff and compact film assembly also due to the rigid polymer backbone with primarily oriented edge-on surface.[27]

Furthermore, Raman spectroscopy was employed to investigate how the biological aqueous environment and the surface coating of poly-L-lysine (PLL), applied prior to cell seeding, affect the BBL film. This technique allowed for detailed examination of the chemical structure and molecular interactions at the film's surface under these conditions (Figure 1D).

One of the primary aspects analyzed was the vibrational modes of the polymer's backbone. Precise attribution of the Raman peaks to specific features of the molecular structure is complex, however collectively they represent vibrational modes of the naphthalene unit (e.g., breathing mode) and the imidazole unit, local vibrations within those units (e.g., specific C═C bonds) as well as more localized vibrations outside the conjugated rings such as the carbonyl or C═N bond. These peaks are sensitive to any changes in molecular structure, such as protonation, oxidation, or the formation of new chemical bonds. The stability of these peaks in the Raman spectra indicated that the BBL polymer did not undergo significant chemical modifications when exposed to the cell culture medium or PLL coating. This suggests that the BBL polymer's intrinsic molecular properties, such as its conjugated structure and electronic characteristics, were preserved.

The results indicated that neither the biological aqueous environment nor the application of the PLL coating caused any significant changes to the material's chemical properties, such as protonation or other alterations that could impact the film's stability or functionality.

This finding is important because it confirms that the BBL film retains its chemical integrity when exposed to both the cell culture medium and the PLL coating.

The PLL adsorption process was further monitored using quartz crystal microbalance with dissipation monitoring (QCM-D). The QCM-D sensorgram reported in **Figure** 2A shows a high frequency overtones spread for PLL adsorbed on BBL film likely due to the percolation of proteins within the polymer layer.[26,27]

Additionally, a significant frequency shift and corresponding mass uptake were observed, suggesting that the high surface roughness may enhance mass adsorption. Notably, no significant desorption occurred after rinsing, indicating that PLL remains stably adsorbed and assembled on the polymer surface. After adsorption reached a steady state, the frequency (Δf) and dissipation (ΔD) shifts were measured. Given the low dissipation value, indicating a rigid layer, the Sauerbrey equation was applied to calculate the adsorbed mass and the number of molecules on the surface (Table S2, Supporting Information).

By analyzing the mass uptake plot in Figure 2B, the kinetics of PLL adsorption were studied. The apparent diffusion coefficient (S), representing the rate at which molecules diffuse to the surface, and the average mass transfer rate constant (kc), which reflects the efficiency of convection-driven protein transport and binding, were calculated. The results show fast adsorption kinetics, confirming a strong affinity and interaction of PLL with the BBL surface (Table S2, Supporting Information).

Next, we examined the adsorption of Dulbecco's Modified Eagle medium (DMEM) cell medium, supplemented with fetal bovine serum (FBS), L-glutamine (L-Glu), and penicillin-streptomycin (PS), onto the BBL film. In this case, the spread of frequency overtones was negligible (Figure S3A, Supporting Information), suggesting the formation of a more rigid film. Notably, DMEM exhibited significantly greater adsorption compared to PLL (Figure S4, Supporting Information). In fact, the adsorbed mass of DMEM on BBL was approximately 5.5 times higher than that of PLL, likely due to the larger number of binding species present in the DMEM formulation (Table S3, Supporting Information).

The kinetic constants, calculated based on the diffusion-driven step of the adsorption process (Figure S4B, Supporting Information), showed an apparent diffusion coefficient (S) similar to that of PLL adsorption. However, the higher value of the average mass transfer rate constant (kc) indicates faster adsorption kinetics for DMEM compared to PLL on BBL (Table S3, Supporting Information).

The cytotoxicity of both pristine and PLL-coated BBL films was assessed by culturing HT22 cells for 2 d in vitro (2 DIV) (Figure S5, Supporting Information). Live (Calcein AM, λ_{ex} 496 nm, λ_{em} 516 nm) and dead cells (ethidium homodimer, λ_{ex} 528 nm, λ_{em} 617 nm) were labeled and visualized (**Figure** 3Ai,ii, Figure S5, Supporting Information). Statistical analysis was conducted to evaluate cell viability, expressed as the live-to-dead cell ratio (Figure 3B). Remarkably, cell viability was high in all conditions, exceeding 93% (control substrate micrographs in Figure S6, Supporting Information).

These findings were further supported by the MTT proliferation assay, which measures cell activity by quantifying the production of formazan, a substance generated by metabolically active cells thus reflecting cell viability. The amount of formazan is

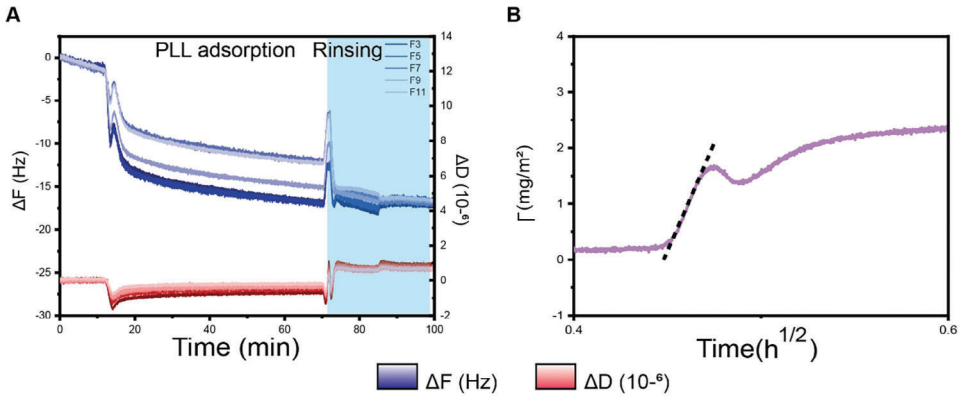

Figure 2. QCM-D sensorgram. A) Quartz crystal microbalance with dissipation monitoring (QCM-B) sensorgram representing all frequency overtones (in blue) and dissipation overtones (in red) related to PLL adsorption, B) related to adsorption kinetics onto BBL.

determined by measuring absorbance at approximately 570 nm, with higher levels indicating greater cell viability. The test showed that cells cultured on BBL films were as healthy and active as those in the control samples (Figure 3C, Experimental Section).

To further assess the film–cell biointerface, key indicators such as adhesion, spreading, and stretching on the surface were evaluated.[28] Cell adhesion is a critical measure of biocompatibility, indicating the cells' ability to attach and survive on a material.[29,30] Beyond adhesion, cell spreading shows that the cells not only attach but also extend and adopt a functional morphology, which is essential for proliferation. Stretching, or the elongation of cells in response to mechanical cues from the surface, further reflects cell health and the material's capacity to support cellular functions. This behavior is linked to cytoskeletal reorganization in response to the material's topographical features.

Here, F-actin, a fundamental component of the cytoskeleton, plays a major role in maintaining cell shape and facilitating adhesion while focal adhesions support the F-actin stress fibers connection to the extracellular matrix (ECM), and assemble as protein complex regulating cellular attachment and mechanical signaling. In particular, it acts as a scaffold by recruiting other proteins and linking integrins to the actin cytoskeleton

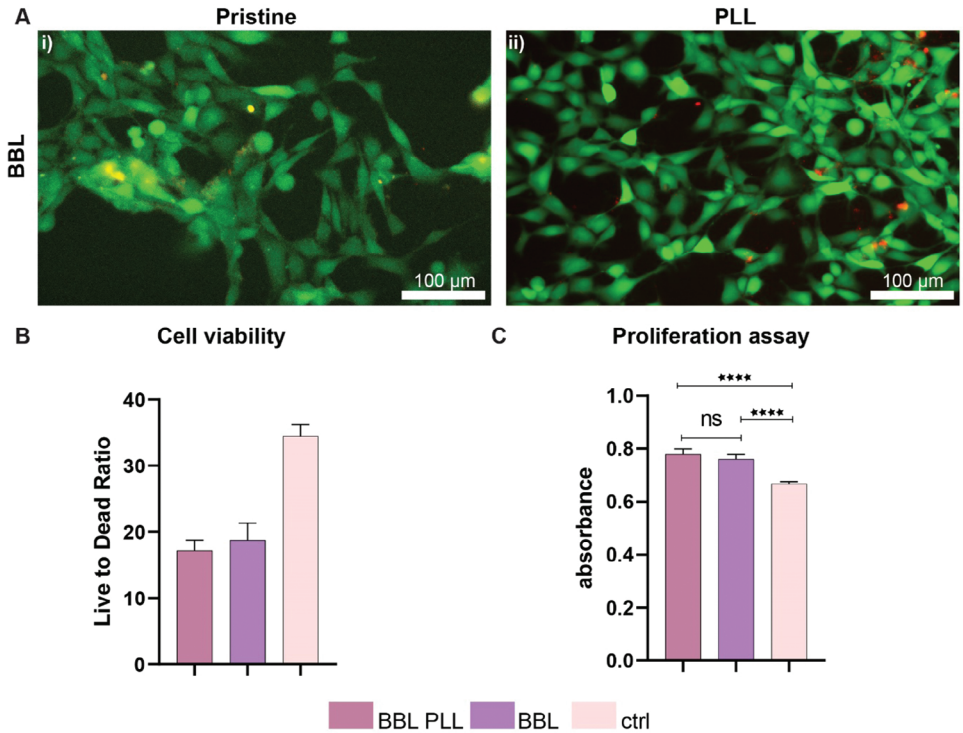

Figure 3. Biocompatibility and proliferation assay of HT22 cells cultured on BBL polymer films. A) HT22 cells cultured on i) pristine, ii) PLL-coated BBL film showing live (green) and dead (red) cells, B) statistical analysis of displaying the percentage of the live and dead cells populations ratio reported as mean ± SD ($n = 3$). C) MTT assay showing cell proliferation in terms of absorbance, on BBL film (pristine and PLL-coated) ($p < 0.05$, $n = 3$).

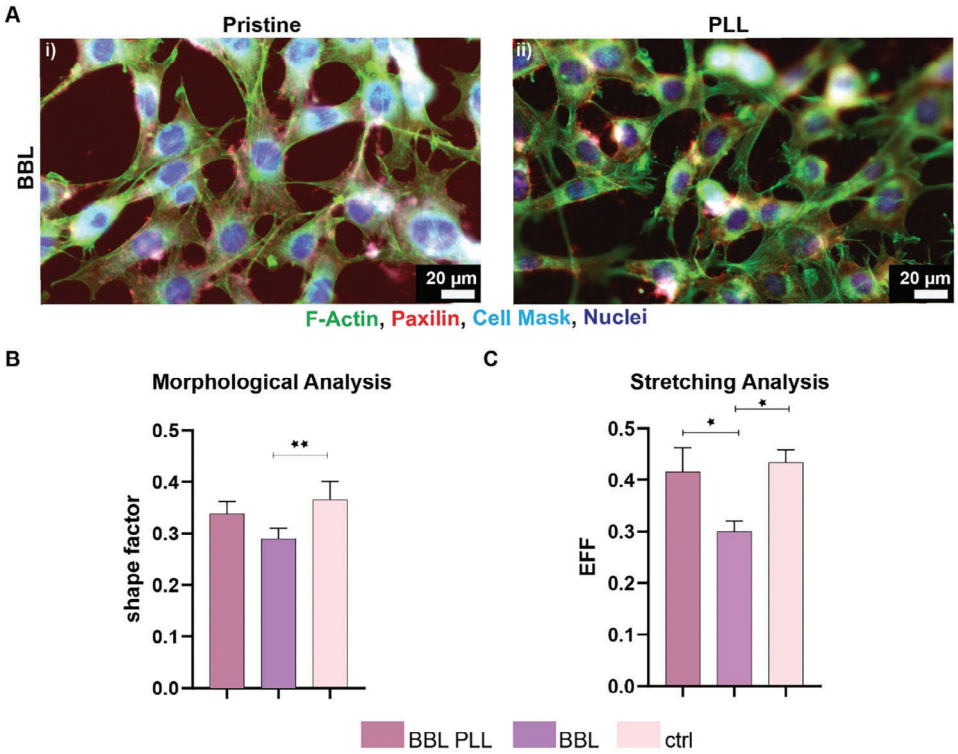

Figure 4. Morphological characterization of HT22 cells cultured on BBL polymer films. A) F-actin (green), paxillin (red) cell membrane (light blue) and nuclei (blue) labelling in HT22 cells cultured on i) BBL, ii) BBL PLL-coated. Morphological analysis in terms of B) shape factor reported as mean ± SD, mixed effect analysis, $*p < 0.05$. Stretching analysis in terms of C) elliptical form factor (EFF) reported as mean ± SD, one-way ANOVA test, $**p < 0.05$, $*p < 0.05$.

to stabilize cell adhesion.[31] The interplay between F-actin and paxillin is essential for the formation and maturation of focal adhesions, which is crucial for effective cell spreading and proliferation.

The ability of cells to adhere, spread, and stretch in response to surface cues provides insights into the material's biocompatibility. Cytoskeletal reorganization, particularly involving F-actin and Paxillin, reflects how well cells interact with the material, directly impacting their viability and function (**Figure 4**).

These evaluations were performed on both uncoated (pristine) and protein-coated (PLL) BBL samples (Figure 4Ai,ii) to determine the material's impact on cellular behavior. The results showed that focal adhesion proteins formed larger nucleation sites on BBL substrates, likely due to the high surface roughness. This suggests that the rough BBL surface enhances focal adhesion formation, potentially strengthening cell-matrix interactions. Additionally, F-actin and membrane labeling revealed effective cell spreading, indicating proper cytoskeletal organization and membrane extension (control substrates in Figure S7, Supporting Information). These findings underscore the significant role of surface topography in shaping cellular behavior, suggesting potential benefits of using BBL substrates in applications that require strong cell adhesion and biocompatibility.

These adhesion sites might also determine the effective spreading area and elongation of cells, which was further analyzed by calculating shape and elliptical form factors. The shape factor was calculated as $4\pi A/P^2$, where A represents the area and P is the perimeter. This factor indicates cell roundness, with values ranging from 0 to 1, where 1 represents a perfectly round cell.[28] The results suggest that uncoated BBL film surfaces influence cell morphology, making the cells rounder (Figure 4B). Additionally, the elliptical form factor (EFF), defined as the ratio of the minor to the major axis of an ellipse fitted to the cell perimeter, revealed significant deformation in cell morphology on an uncoated polymer surface compared to the control samples (Figure 4C).

To further investigate the cell–material interface at adhesion sites, fixed and embedded cells[8,29] on BBL films were sectioned using a focused ion beam and imaged with a scanning electron microscope (**Figure 5**A,B). This advanced imaging technique allowed for high-resolution visualization of the interaction between the cell membrane and the underlying BBL films. The micrographs showed that the plasma membrane (green line) maintains close adherence to the surface of the film, irrespective of the surface's functionalization. This strong adhesion suggests that surface chemistry, whether pristine or PLL coated, does not substantially alter the membrane's ability to form intimate contact with the substrate. This observation can imply that the physical characteristics of the BBL films, such as nanoscale topography and stiffness, may play a more prominent role in dictating cell behavior at these adhesion points. Additionally, the surface roughness of the BBL film (pink line) appeared to promote membrane ruffling, as evidenced by the presence of membrane invaginations and protrusions at the interface.[32] These ruffles likely serve as anchoring points for the cells, and this could indicate that the nanoscale roughness of the substrate fosters a more dynamic and

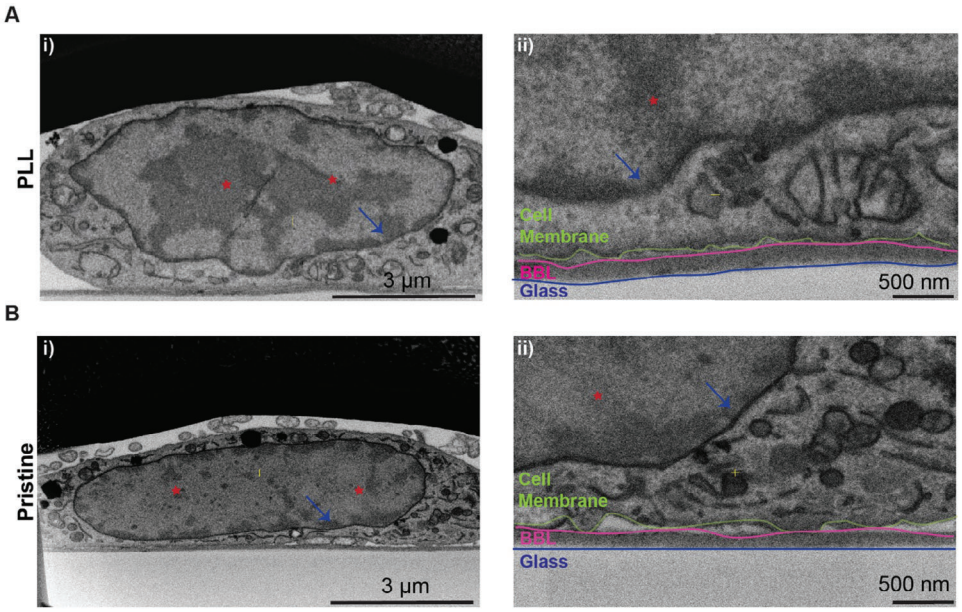

Figure 5. Interaction between HT22 cell line on BBL polymer films. A) scanning electron micrographs showing the interaction between HT22 cells on PLL coated BBL at i) low magnification and ii) high magnification and B) pristine BBL at i) high magnification and ii) low magnification. These micrographs highlight the interaction between the cell membrane (green line) and the BBL film (pink line). Red stars indicate the nucleus, and the blue arrows indicate the nuclear membranes.

robust interaction between the cell and the material, promoting cellular processes supporting cellular growth and function.

3. Conclusions

In this study, we provided a comprehensive evaluation of the biocompatibility and cell interaction properties of the benchmark n-type mixed conductor BBL, demonstrating its potential as platforms for neuronal culture and bioelectronic interfaces. BBL films exhibit high surface roughness and stiffness, which enhance their stability in biological media and resistance to degradation during cell culture. These characheristics are essential for preserving material integrity in long-term bioelectronic applications.

Protein adsorption studies revealed that BBL films exhibit a high mass uptake of poly-lysine (PLL), suggesting strong interactions with proteins. This increased adsorption is likely due to the surface roughness of BBL, which facilitates effective protein binding. Additionally, BBL films, whether pristine or coated with PLL, supported high cell viability, with over 93% of cells remaining viable across all conditions. Cell proliferation assays further confirmed that cells cultured on BBL films were as healthy and active as those on control substrates, demonstrating the non-cytotoxic nature of both materials.

This study also found that BBL's rougher surface promoted larger focal adhesion formation and improved cytoskeletal organization, enhancing cell adhesion and spreading. Analysis of cell shape and elliptical form factors revealed that uncoated BBL films significantly influenced cell morphology.

Overall, surface roughness emerged as a key factor influencing cell–matrix interactions, with the rough BBL surface promoting strong cell anchoring and adhesion. These results position BBL as a promising material for bioelectronic applications, particularly in neuroelectronics, due to its enhanced protein adsorption, excellent biocompatibility, and ability to support robust cellular adhesion and proliferation. Additionally, its stability in aqueous environments highlights its potential for long-term interfacing with neuronal cells in bioelectronic devices.

4. Experimental Section

Films' Deposition and Manufacturing: Glass slides (1.5 × 1.5 cm^2) were cleaned by sequential sonication in acetone, deionized water, and isopropanol. They were then dried with a nitrogen flow and further cleaned with oxygen plasma (Zepto-W6 by Diener electronic). The cleaned glass slides were coated with a 5 µm thick layer of parylene C (Sigma-Aldrich) with the assistance of silane A174 (Sigma-Aldrich). BBL was synthesized following the procedure reported in ref. [22] In brief, PPA (250 g, 3.13 mol) was deoxygenated overnight at 110 °C under nitrogen. TABH (2.00 g, 7.05 mmol) was added at 50 °C. The mixture was heated overnight at 75 °C, and NDA (1.89 g, 7.05 mmol) was then added. The mixture was heated to 180 °C for 12 h to yield BBL (M_v = 28.4 kDa). The resulting viscous solution was poured into a beaker, cooled, and precipitated in methanol. The brown fibrous material was washed with methanol and water and then dried at 200 °C under reduced pressure. BBL was then dissolved in methanesulfonic acid (MSA) to obtain a solution with a concentration of 3–5 mg mL^{-1}, which was spin-coated onto the glass/Parylene substrates at 1000 rpm for 30 sec. The BBL thin films were subsequently immersed in deionized water for 5 min to eliminate residual MSA and dried with a nitrogen flow to achieve ≈50 nm thin films.

Atomic Force Microscopy: Atomic force microscopy (AFM) measurements were carried out in tapping mode (TM) by using a Nanoscope IIIA-MultiMode AFM (Digital Instruments-DI, Santa Barbara, CA, USA). The device was equipped with a <J> calibrated scanner using grating manufacturers. The surface morphology of pristine BBL film and PLL-coated BBL film, obtained after 1 h incubation in poly-L-lysine (Mw 70000–150000 Da) at a concentration of 0.01% w/v (Sigma- Aldrich) followed by two rins-

ing steps in PBS and the final step in MilliQ water was evaluated both in air and in liquid (PBS), images in air were recorded at scan rate of 1 Hz and 512 × 512 pixels per image (i.e., in high resolution conditions) by using 0.5–2 Ω cm phosphorous (*n*) doped silicon tips mounted on cantilevers with a nominal force constant of 40 N m^{-1} and a resonant frequency of 300 kHz (model Tap300-G, BudgetSensors, Bulgaria). The force was maintained at the lowest possible value by continuous adjusting the set point during imaging. Images in liquid were acquired in tapping mode using a fluid cell filled with phosphate buffer saline (PBS) solution. Sharpened silicon nitride probes with a nominal force constant of 0.24 N m^{-1} and a resonant frequency of 56 kHz (model DNP-S10, Bruker, USA) were employed.

Image analysis was carried out using DI software, version 4.23r6. The images were flattened to remove background slopes.

Film roughness was measured on TM images obtained at a scan speed of 1 Hz over scanned areas of 2 × 2 mm^2 for a minimum of six separate zones for each sample obtained from different regions. The roughness values are expressed in terms of R_a, R_q, and R_{max}. R_a expresses the arithmetic average of the absolute values of the surface height deviations measured from the mean plane within the cursor box using the Equation 1:

$$R_a = \frac{1}{n}\sum_{j=1}^{n}\left|Z_j\right| \tag{1}$$

R_q is the standard deviations of the *Z* values and is calculated as (Equation 2):

$$R_q = \sqrt{\frac{\sum (Z_i)^2}{n}} \tag{2}$$

where the current *Z* value and *n* is the number of points within the cursor box. Finally, R_{max} is the maximum vertical distance between the highest and lowest data points within the cursor box.

The Young's modulus was calculated from the collected force–distance curves measured with the NTEGRA AFM (NT-MDT, Moscow, Russia). Stiff single-crystal silicon cantilevers with a symmetric tip shape were used (model Tap300Al-G, BudgetSensors, Bulgaria: nom. Frequency 300 kHz, nom. Spring constant 40 N m^{-1}, tip radius < 10 nm). The probe was characterized by measuring the cantilever spring constant by the Sader method.[31] Each probe was calibrated by performing a force curve on a hard-cleaned substrate (<100> silicon wafer), to calculate the sensitivity. The Young's modulus was obtained from the experimental force–distance curves, considering the elastic region by the Derjaguin–Müller–Toporov (DMT) model[32] using the following Equation 3:

$$F + F_{ad} = \frac{4E_s}{3\left(1-\nu_s^2\right)} R^{(1/2)}\delta^{(3/2)} \tag{3}$$

where *F* is the applied force; F_{ad} is the adhesion force; E_s is Young's modulus; ν_s is the Poisson's ratio for the sample; *R* is the radius of the spherical indenter; and δ is the elastic indentation depth. The measurements were made in triplicate and each surface was indented in different areas, acquiring five hundred curves for sample. The nanoindentation was performed from 500 to -50 nm. Young's modulus was calculated by fitting experimental curves with the DMT model in the elastic region.

Scanning Electron Microscopy of Films: The surface of the BBL films was observed by mounting the films onto aluminum stubs (Sigma-Aldrich, cat. Num. 933155-1EA, diameter 3.2 mm), using conductive paste (RS Pro, cat. Num. 123-9911), and then sputtered with 7 nm of gold. Afterwards, they were loaded inside the vacuum chamber of a dual FIB-SEM machine (Thermofisher, Helios CX 5) and the imaging was performed by using the electron beam. Firstly, a top view was captured, current of 0.17 nA and tension of 3 kV, with a dwell time of 20 µs. Then, the stage was also positioned at 52° at micrographs were acquired with a current of 0.17 nA, voltage 3 kV and dwell time of 20 µs.

Sample Preparation for Cell Culture: Films were sterilized in a laminar flow sterile hood (for cell culture) with UV for 1h. Then, they were immersed in 70% v/v EtOH (Merck Life Science S.r.l., Italy, cat. num. 24105-2.5L-M) for 20 min, followed by three washes with autoclaved MilliQ water and drying under the hood. Prior to cell plating, films were treated for the adsorption of Poly-L-lysine (Mw 70 000–150 000 Da) at a concentration of 0.01% w/v (Sigma- Aldrich). After 1 h of incubation at 37 °C, the protein coating was removed, and the films were washed with warmed in supplemented Dulbecco's modified Eagle medium—Nutrient mixture F-12 media.

Neuronal Cell Culture: HT22 are mouse hippocampal neuron-derived cells (gifted from Velia Siciliano's lab, Istituto Italiano di Tecnologia, Italy); they were cultured in Dulbecco's modified Eagle medium—Nutrient mixture F-12 media (DMEM—F12, Merck Life Science S.r.l., Italy), supplemented with 10% fetal bovine serum (FBS, Life Technologies Italia, Italy), 1% L-glutamine (Merk Life Science S.r.l., Italy). The medium was changed every three days. When 90% confluence was reached, HT22 were detached by adding 1 mL of 0.25% trypsin-EDTA (Life Technologies, Italy, cat. Num. 25200072) for 5 min in the incubator, and then they were collected in 5 mL of warm media. The cell suspension was then centrifuged at 1000 rpm for 5 min. Then, the supernatant was removed, and the cells were resuspended in 1 mL of warm supplemented media prior to cell counting carried out with trypan blue stain 0.4% (Invitrogen, Thermo Fisher Scientific, USA). 10 µL of warm supplemented media with cells were mixed with 10 µL of Trypan blue and then the cells were counted by using the cell counting chamber (Thermo Fisher Scientific, cat. Num. C10228) and the benchtop The Countess 3 Automated Cell Counter (ThermoFischer Scientific). Cells were then plated at a density of 36 000 cells cm^{-2} on the different films.

Quartz Crystal Microbalance with Dissipation Monitoring: Measurements of adsorption kinetics were performed by using a Quartz Crystal Microbalance with Dissipation Monitoring (QCM-D) instrument (Q-Sense AB, Sweden) with AT-cut gold crystals sensors. The measurement chamber was operating in buffer saline (outgassed with 30 min sonication) at 25 ± 0.1 °C and the flow rate was 100 µL min^{-1}. The simultaneous measurements of frequency, *f* and energy dissipation, *D*, were performed for the fundamental resonance frequency ($n = 1$, i.e., $f \approx 5$ MHz) and the six overtones ($n = 3, 5, 7, 9, 11$ and 13 corresponding to $f \approx 15$, ≈ 25, ≈35, ≈45, ≈55, and ≈65 MHz, respectively). In case of rigid, evenly distributed and sufficiently thin adsorbed layers, the frequency-to-mass conversion was simply obtained by using Sauerbrey equation (Equation 4):

$$M = -\left(\frac{C}{n}\right) f \tag{4}$$

here *f* is the decrease in resonant frequency, *M* is the mass uptake at the sensor surface, *C* is a constant depending on the intrinsic properties of quartz slab (in our case $C = 17.7$ ng cm^{-2} Hz^{-1} at $f = 5$ MHz) and n is the overtone number. The resolution in *f* and *D* is ±0.1 Hz and 1×10^{-7},[33] respectively.

Each QCM-D experiment started with the sensor running stable in buffer solution for 10 min, then, the addition of 400 µL PLL or DMEM solution, and the protein adsorption process is followed for 1 h, then the exchange of the protein solution with PBS solution at minutes 70 and 85, to rinse the surface and to check both desorption of molecules not attached to the surface and stability of the adsorbed layer.

Poly-L-Lysine (PLL) and Dulbecco's modified eagle medium (DMEM high glucose, no glutamine, no phenol red) medium were purchased respectively by Sigma-Aldrich and Merck Life Science S.r.l., Italy. PLL solution 0.01% w/v sterile filtered, average *M*w 70000–150000 Da, was used as purchased. The DMEM complete medium was prepared adding 10% v/v of fetal bovine serum (FBS, Life Technologies Italia, Italy), 1% v/v of penicillin–streptomycin (PS, Merk Life Science S.r.l., Italy) and 1% v/v of L-glutamine (L-glu, Merk Life Science S.r.l., Italy) to the commercial DMEM. For PLL adsorption measurements, phosphate-buffered saline (PBS) tablet (Sigma Aldrich) dissolved in MilliQ water was used as baseline, for DMEM adsorption a buffer solution prepared with inorganic salts present in DMEM

formulation, buffered at pH 7.4 was prepared. All the QCM-D measurements were performed in triplicate and the data are presented as mean ± SD calculated considering all the overtones for each measurement.

The random sequential adsorption (RSA) analysis allows to calculate the apparent diffusion coefficient (S) and the related average mass transfer rate constant (k_c) for the protein adsorption. The coefficient S can be calculated from the slope of the diffusion-controlled step, considering Equation 5:

$$\Gamma\ (t) = \frac{2}{\sqrt{\pi}}\sqrt{St}C_{\text{bulk}} \tag{5}$$

in which Γ is the mass uptake, C is the bulk concentration, and t is the time.

Instead, the constant k_c describes the efficiency of the convection-driven protein mass transport and binding to the surfaces, and it can be calculated from Equation 6:

$$k_c = C_f\ Q^{\frac{1}{3}} S^{\frac{2}{3}} \tag{6}$$

where Q is equal to 1.7×10^{-3} cm^3 s^{-1} and corresponds to the volumetric flow rate used for the measurements, $C_f = 19.9$ cm$^{-4/3}$ is a constant that depends on geometrical factors of the QCM-D cell and is independent from solution concentration, molecule size and flow rate, and S is the diffusion coefficient previously calculated. The kinetic parameters were obtained by using the more sensitive frequency overtone ($F3$).

Raman Spectroscopy: BBL was spin coated at 1000 rpm for 60 s on glass slides coated with silane A174 and parylene C. The samples were subsequently rinsed with ethanol (70% v/v) and MilliQ water. The dry film was first measured and then the samples were incubated in a poly-L-lysine (PLL) solution (0.01% w/v) for 1 h. After this was done, the samples were placed in Dulbecco's modified eagle medium (DMEM) and measured in Raman while in contact with the DMEM solution. Spectra were acquired in the Raman Stokes region using 532 nm excitation wavelength, in the range 1000–1800 cm^{-1} (Horiba LamRAM Evolution Confocal Raman). A 100x LWD Olympus objective was used to perform measurements with laser power set at <0.963 mW to avoid sample degradation. For a good signal-to-noise ratio, each spectrum was taken over an integration time of 20 s and averaged over three measurements. The spectrometer was calibrated through a Si sample using the spectral line 520.7 cm^{-1}. Spectra were analyzed using LabSpec 6 software.

Biocompatibility and Proliferation Assays: Biocompatibility assay was carried out with Calcein acetoxymethyl (Calcein-AM, Merck Life Science S.r.l., Italy) at a concentration of 1:1000 in phosphate buffered saline (PBS, Sigma-Aldrich cat. num. P4417-100TAB) to label live cells, and 1 µg mL^{-1} ethidium homodimer (Sigma Aldrich, cat. num. 46043) was added and then incubated for 15 min at 37 °C. After 2 DIV, cells' media was removed and cells were rinsed with warm PBS and then incubated with the staining solution for 15 min at 37 °C, 5% CO_2, and 95% humidity. Afterwards, samples were washed with warm PBS and image acquisition was performed with anAxiobserver-Z1 microscope (Zeiss, Germany) equipped with 20x water immersion lens. Image-J software was utilized for quantifying the number of live and dead cells, and the percentage of live cells was calculated employing the following formula (Equation 7):

$$\%\text{viability} = \frac{(\text{Livecells})}{(\text{livecells} + \text{Deadcells})} \cdot 100 \tag{7}$$

A proliferation assay was carried out using MTT thiazolyl blue tetrazolium bromide (Abcam, num. Cat. ab146345-1 g, 5 mg mL^{-1} in PBS).

Each sample placed in a 24-multiwell was incubated with 0.5 mL of warm media and 0.2 mL of MTT solution for 3.5 h. Afterwards the media was completely removed and 1 mL of dimethyl sulfoxide hybri-max sterile-filt DMSO (Merk Life Science S.r.l., Italy) was added and incubated for 1 h under dark conditions. Subsequently, 0.2 mL of solution was transferred into a 96-multiwell, (with each well corresponding to three smaller wells). Absorbance was measured at 570 nm using a spectrophotometer.

Each experimental condition was studied in triplicate ($n = 3$).

Immunohistochemistry: Cells were fixed after 2 DIV in culture using a solution of 4% v/v paraformaldehyde (PFA) (Sigma–Aldrich) for 20 min at room temperature (RT). After rinsing three times in PBS permeabilization was carried out by incubating in 0.1% v/v Triton-X 100 (Sigma-Aldrich cat. num. T9284-1L) for 5 min.

Blocking solution was prepared with 2% w/v bovine serum albumin (BSA, Sigma–Aldrich) in PBS and melted at RT. The samples were immersed in the blocking solution for 45 min at RT to enhance the assay.

Immunohistochemistry was performed by labeling paxillin using a primary antibody (mouse, Thermo Fisher Scientific, cat. num. AHO0492) at a 1:200 dilution in 2% BSA in PBS for 1 h at RT. Cells were then incubated with Alexa Fluor 546 (1:500 in 2% w/v BSA, Thermo Fisher Scientific, cat. num. A11030) for 30 min. The samples were rinsed three times for 5 min each in 2% w/v BSA. Subsequently, phalloidin-X 488 conjugated dyes (1:1000 dilution in 2% w/v BSA, Sigma-Aldrich, cat. num. D8537) were applied for 1 h at RT. After washing three times, Hoechst was used at a 1:5000 dilution in PBS (Thermo Fisher Scientific, cat. num. H3570) for 5 min at RT.

The cells were then incubated for 15 min in CellMask Deep Red (1:1000 in PBS, Thermo Fisher Scientific, cat. num. C10046). Finally, the samples were washed three times with PBS.

Afterwards, the samples underwent a thorough PBS wash and were imaged using an Axio Observer Z1 microscope (Zeiss, Germany) equipped with a 20x water immersion lens and 1.5x magnification. ImageJ software (NIH, USA) was used to process the images.

Morphological Analysis: Cell morphological features were considered defining the shape factor as $4\pi A/P^2$, where A is the area and P is the perimeter of the cell; the elliptical form factor (EFF), determined by the ratio of the major axis to the minor axis and the average area covered by the cell. Measurements involving cell area, perimeter, minor and major axis length were conducted using ImageJ (NIH, USA).[28]

Ultra-Thin Resin Embedding (UTP) of Specimens: Samples underwent an ultrathin plasticization (UTP) procedure based on as previously reported.[34]

Briefly, samples were fixed in a 2.5% v/v glutaraldehyde solution (Società Italiana Chimici, Italy) diluted in a 0.1 M sodium cacodylate buffer solution (Società Italiana Chimici, Italy) overnight at 4 °C. After the overnight incubation, samples were rinsed in 0.1 M sodium cacodylate buffer solution three times for 5 min (each step) and then they were kept for 20 min at 4 °C in a 20 mM glycine solution in 0.1 M sodium cacodylate (Merck Life Science S.r.l., Italy). Afterwards the cells were incubated for 1 h at 4 °C in a solution of 4% v/v osmium tetroxide (Electron Microscopy Science) and 2% v/v potassium ferrocyanide, both diluted in 0.1 M sodium cacodylate (Electron Microscopy Science) under dark conditions. Samples were then washed three times with 0.1 M cacodylate buffer solution, 4 °C. Carefully, the specimens were rinsed three times, each for 5 min, with MilliQ water solution at room temperature and then immersed in 1% w/v filtered thiocarbohydrazide (TCH, Electron Microscopy Science) in DI water for 20 min at room temperature. A final incubation of 2% v/v osmium tetroxide (Electron Microscopy Science) aqueous solution was performed at room temperature, 30 min. Subsequently the samples were washed three times in MilliQ water, each for 5 min, and then they were incubated overnight at 4 °C with en bloc staining solution (4% v/v uranyl acetate in MilliQ water). After rinsed the samples three times in DI water, they were kept for 3 min in 0.15% w/v tannic acid solution (Sigma Aldrich) at 4 °C. Then the dehydration was carried out in a series of ethanol dilutions (30% v/v, 50% v/v, 75% v/v, 2 × 95% v/v, 100% v/v, ethanol in water) each for 10 min at 4 °C. In addition, 100% ethanol was exchanged twice at RT, each for 10 min. Finally, the sample were gradually embedded in resin (25 mL of NSA, 8 mL D.E.R. 736, 10 mL of ERL 4221, 301 µL DMAE, Electron Microscopy Science) with different ethanol:resin ratios. The first embedding was in ethanol:resin with a ratio 1:3 and the samples were kept embedded for 2 h, then the second ratio 1:2, for 2 h and then 1:1 overnight at room temperature. Afterwards, the samples were placed in a 2:1 mixture of resin and ethanol for 2 h. Then, the final embedding was done in pure resin, and the samples were left in this solution overnight and throughout the following day. Finally, specimens were kept in a vertical position for 3 h

and then polymerized for 24 h at 70 °C. Then, they were mounted onto aluminum stubs (diameter 3.2 mm) using silver conducting paste (RS Pro) and sputtered with 15 nm thick golden layer prior to imaging.

Scanning Electron Microscopy-Focused Ion Beam of UTP Specimens: The specimens were loaded inside the dual-beam vacuum chamber (Thermo Fisher, Helios CX 5). Then, the region of interest was detected, and a Pt deposition layer were performed by the ion beam deposition (0.5 µm thickness of platinum, with current 0.43 nA and voltage 30 kV). The cross section was carried out by cutting out the material via ion beam milling (depth: 4 µm; current: 0.79 nA; voltage30 kV). The ion beam was then used to polish the interface, current of 0.23 nA; voltage 30 kV. The scanning electron micrographs were acquired in backscattered mode with a dwell time of 20 µs and the electron beam to 3 kV and 0.17 nA.

Data Analysis: AFM images were flattened with the Digital Instrument software version 4.23r6 tool to remove the background slopes and using the same software the roughness analysis was carried out. The roughness averaged values were obtained considering the values obtained for a minimum of six separate zones for each sample from different regions of the substrate. The data were presented as mean ± standard deviation. The Young's modulus was calculated by fitting experimental curves with the DMT model in the elastic region, using the FCprocessor2 of the NovaPx software. Five hundred force–distance curves were acquired indenting each surface in different areas, the measurements were made in triplicate. The presented values were calculated considering the maximum value of the LogNormal distribution of the obtained values.

From the QCM-D experiments, the frequency shift and the dissipation change were obtained by the average of all the overtones recorded, considering the variation between the initial steady state and the values reached after the washing steps at the end of the monitored adsorption. By applying the Sauerbrey equation for the frequency-to-mass conversion, the adsorbed mass was obtained. For PLL adsorption the number of molecules adsorbed per cm^2 was obtained considering the average molecular weight of the protein provided by the company. The data were presented as mean ± standard deviation.

The adsorption kinetic constants were obtained considering the RSA model. The apparent diffusion coefficient (S) was calculated by the slope of the diffusion-controlled step from the plot of the mass uptake calculated for the third overtone of the resonance frequency versus the square root of the adsorption time expressed in hours. The average mass transfer rate constant (k_c) was calculated considering the S value obtained.

Statistical Analysis: For biocompatibility, immunohistochemistry and SEM/FIB experiments, three parallel cultures were prepared for each substrate and every experiment was repeated three times ($n = 3$). The statistical analysis was performed using GraphPad Prisms 8. For the viability assay, a one-way ANOVA test followed by a Tukey's multiple comparisons test was performed to assess any effect of the substrates used on the percentage of live cells compared to glass. For the proliferation assay, a one-way ANOVA test followed by a Tukey's multiple comparisons test was performed to assess any substrate-mediated effect on cell proliferation compared to glass across all culture times investigated. The substrates mediated changes in morphology were compared using Tukey's multiple comparisons test.

Supporting Information

Supporting Information is available from the Wiley Online Library or from the author.

Acknowledgements

C.L.B. and P.C. contributed equally to this work. F.S. and C.L.B. thank Dr. Valentina Mollo for the help providing during the electron microscopy experiments and Dr. Claudia Lubrano and Ms. Daniela Rana for preliminary considerations on cell plating.

Open access funding enabled and organized by Projekt DEAL.

Conflict of Interest

The authors declare no conflict of interest.

Data Availability Statement

The data that support the findings of this study are available from the corresponding author upon reasonable request.

Keywords

BBL, cell-chip coupling, in vitro biocompatibility, neuronal cells, organic bioelectronics

Received: June 1, 2024
Revised: October 13, 2024
Published online: December 23, 2024

[1] M. Berggren, A. Richter-Dahlfors, *Adv. Mater.* **2007**, *19*, 3201.
[2] A. Mariano, C. L. Bovio, V. Criscuolo, F. Santoro, *Nanotechnology* **2022**, *33*, 492501.
[3] S. R. Patel, C. M. Lieber, *Nat. Biotechnol.* **2019**, *37*, 1007.
[4] D. J. Aidley, *The Physiology of Excitable Cells*, Cambridge University Press, Cambridge **1998**.
[5] *Modeling & Imaging of Bioelectrical Activity: Principles and Applications* (Ed: B. He), Springer, New York **2005**.
[6] A. Mariano, C. Lubrano, U. Bruno, C. Ausilio, N. Bhupesh Dinger, F. Santoro, *Chem. Rev.* **2022**, 122, 4, 4552-4580.
[7] F. Corrado, U. Bruno, M. Prato, A. Carella, V. Criscuolo, A. Massaro, M. Pavone, A. B. Muñoz-García, S. Forti, C. Coletti, O. Bettucci, F. Santoro, *Nat. Commun.* **2023**, *14*, 6760.
[8] L. Matino, A. Mariano, C. Ausilio, G. Raghav, T. Cohen-Karni, F. Santoro, *Nano Lett.* **2022**, 22, 21. 8633-8640.
[9] A. J. Hackett, J. Malmström, J. Travas-Sejdicab, *Prog. Polym. Sci.* **2017**, *70*, 18.
[10] L. Almulla, V. Druet, C. E. Petoukhoff, W. Shan, N. Alshehri, S. Griggs, Y. Wang, M. Alsufyani, W. Yue, I. McCulloch, F. Laquai, S. Inal, *Mater. Horiz.* **2024**, *11*, 2937.
[11] P. J. Molino, J. Will, L. Y. Daikuara, A. R. Harris, Z. Yue, J. Dinoro, P. Winberg, G. G. Wallace, *Biointerphases* **2021**, *16*, 021003.
[12] A. Abedi, M. Hasanzadeh, L. Tayebi, *Mater. Chem. Phys.* **2019**, *237*, 121882.
[13] J. R. Aggas, *Biosens. Bioelectron.* **2020**, *168*, 112568.
[14] N. K. Kim, J. W. Bae, H.-K. Jang, J.-C. Lee, K. Song, B.-S. Kim, I. J. Park, J.-W. Ha, S.-B. Lee, E.-H. Sohn, *RSC Adv.* **2016**, *6*, 16540.
[15] V. Druet, D. Ohayon, C. E. Petoukhoff, Y. Zhong, N. Alshehri, A. Koklu, P. D. Nayak, L. Salvigni, L. Almulla, J. Surgailis, S. Griggs, I. McCulloch, F. Laquai, S. Inal, *Nat. Commun.* **2023**, *14*, 5481.
[16] O. Bettucci, G. Maria Matrone, F. Santoro, *Adv. Mater. Technol.* **2022**, *7*, 2100293.
[17] S. Wang, H. Sun, U. Ail, M. Vagin, P. O. Å. Persson, J. W. Andreasen, W. Thiel, M. Berggren, X. Crispin, D. Fazzi, S. Fabiano, *Adv. Mater.* **2016**, *28*, 10764.
[18] A. Babel, S. A. Jenekhe, *J. Am. Chem. Soc.* **2003**, *107*, 1749.
[19] J. Surgailis, A. Savva, V. Druet, B. D. Paulsen, R. Wu, A. Hamidi-Sakr, D. Ohayon, G. Nikiforidis, X. Chen, I. McCulloch, J. Rivnay, S. Inal, *Adv. Funct. Mater.* **2021**, *31*, 2010165.
[20] A. V. Volkov, H. Sun, R. Kroon, T.-P. Ruoko, C. Che, J. Edberg, C. Müller, S. Fabiano, X. Crispin, *ACS Appl. Energy Mater.* **2019**, *2*, 5350.

[21] H. Wu, C. Yang, Q. Li, N. B. Kolhe, X. Strakosas, M. Stoeckel, Z. Wu, W. Jin, M. Savvakis, R. Kroon, D. Tu, H. Y. Woo, M. Berggren, S. A. Jenekhe, S. Fabiano, *Adv. Mater.* **2022**, *34*, 2106235.
[22] C.-Y. Yang, D. Tu, T.-P. Ruoko, J. Y. Gerasimov, H.-Y. Wu, P. C. Harikesh, R. Kroon, C. Müller, M. Berggren, S. Fabiano, *Adv. Electron. Mater.* **2022**, 8, 2100907.
[23] H.-Y. Wu, J.-D. Huang, S. Y. Jeong, T. Liu, Z. Wu, T. Van Der Pol, Q. Wang, M.-A. Stoeckel, Q. Li, M. Fahlman, D. Tu, H. Y. Woo, C.-Y. Yang, S. Fabiano, *Mater. Horiz.* **2023**, *10*, 4213.
[24] P. C. Harikesh, C.-Y. Yang, H.-Y. Wu, S. Zhang, M. J. Donahue, A. S. Caravaca, J.-D. Huang, P. S. Olofsson, M. Berggren, D. Tu, S. Fabiano, *Nat. Mater.* **2023**, *22*, 242.
[25] P. C. Harikesh, C.-Y. Yang, D. Tu, J. Y. Gerasimov, A. M. Dar, A. Armada-Moreira, M. Massetti, R. Kroon, D. Bliman, R. Olsson, E. Stavrinidou, M. Berggren, S. Fabiano, *Nat. Commun.* **2022**, *13*, 901.
[26] C.-Y. Yang, M.-A. Stoeckel, T.-P. Ruoko, H.-Y. Wu, X. Liu, N. B. Kolhe, Z. Wu, Y. Puttisong, C. Musumeci, M. Massetti, H. Sun, K. Xu, D. Tu, W. M. Chen, H. Y. Woo, M. Fahlman, S. A. Jenekhe, M. Berggren, S. Fabiano, *Nat. Commun.* **2021**, *12*, 2354.
[27] T. Liu, J. Heimonen, Q. Zhang, C.-Y. Yang, J.-D. Huang, H.-Y. Wu, M.-A. Stoeckel, T. P. A. van der Pol, Y. Li, S. Y. Jeong, A. Marks, X.-Y. Wang, Y. Puttisong, A. Y. Shimolo, X. Liu, S. Zhang, Q. Li, M. Massetti, W. M. Chen, H. Y. Woo, J. Pei, I. McCulloch, F. Gao, M. Fahlman, R. Kroon, S. Fabiano, *Nat. Commun.* **2023**, *14*, 8454.
[28] A. Mariano, I. Fasolino, N. B. Dinger, C. Latte Bovio, I. Bonadies, A. Pezzella, L. Ambrosio, M. G. Raucci, F. Santoro, *Adv. Mater. Interfaces* **2023**, *10*, 2202022.
[29] M. Ventre, F. Causa, P. A. Netti, *J. R. Soc., Interface* **2012**, *9*, 2017.
[30] M. Ventre, P. A. Netti, *ACS Appl. Mater. Interfaces* **2016**, *8*, 14896.
[31] K. Lee, E. H. Kim, N. Oh, N. A. Tuan, N. H. Bae, S. J. Lee, K. G. Lee, C.-Y. Eom, E. K. Yim, S. Park, *J. Nanobiotechnol.* **2016**, *14*, 35.
[32] W. Zhao, L. Hanson, H.-Y. Lou, M. Akamatsu, P. D. Chowdary, F. Santoro, J. R. Marks, A. Grassart, D. G. Drubin, Y. Cui, B. Cui, *Nat. Nanotechnol.* **2017**, *12*, 750.
[33] M. Rodahl, F. Höök, B. Kasemo, *Anal. Chem.* **1996**, *68*, 2219.
[34] F. Santoro, W. Zhao, L.-M. Joubert, L. Duan, J. Schnitker, Y. van de Burgt, H.-Y. Lou, B. Liu, A. Salleo, L. Cui, Y. Cui, B. Cui, *ACS Nano* **2017**, *11*, 8320.